Atmos. Chem. Phys. Discuss., 12, 24643–24676, 2012
www.atmos-chem-phys-discuss.net/12/24643/2012/
doi:10.5194/acpd-12-24643-2012

Atmospheric Chemistry and Physics Discussions

An assessment of CALIOP polar stratospheric cloud composition classification

M. C. Pitts[1], L. R. Poole[2], A. Lambert[3], and L. W. Thomason[1]

[1]NASA Langley Research Center, Hampton, Virginia 23681, USA
[2]Science Systems and Applications, Incorporated, Hampton, Virginia 23666, USA
[3]Jet Propulsion Laboratory, California Institute of Technology, Pasadena, California 91109, USA

Received: 15 August 2012 – Accepted: 4 September 2012 – Published: 20 September 2012

Correspondence to: M. C. Pitts (michael.c.pitts@nasa.gov)

Published by Copernicus Publications on behalf of the European Geosciences Union.

Abstract

This study assesses the robustness of the CALIOP (Cloud-Aerosol Lidar with Orthogonal Polarization) polar stratospheric cloud (PSC) composition classification algorithm – which is based solely on the spaceborne lidar data - through the use of nearly coincident gas-phase HNO_3 data from the Microwave Limb Sounder (MLS) on Aura and Goddard Earth Observing System Model, Version 5 (GEOS-5) temperature analyses. Following the approach of Lambert et al. (2012), we compared the observed temperature-dependent HNO_3 uptake by CALIOP PSCs with modeled uptake for equilibrium STS (supercooled ternary solution) and NAT (nitric acid trihydrate), which indicates how well PSCs in the various composition classes conform to expected temperature existence regimes and also offers some insight into PSC growth kinetics. We examined the CALIOP PSC data record from both polar regions over the period from 2006 through 2011 and over a range of potential temperature levels spanning the 15–30 km altitude range. We found that most PSCs identified as STS exhibit gas phase uptake of HNO_3 consistent with theory, but with a small temperature bias, similar to Lambert et al. (2012). Ice PSC classification is also robust in the CALIOP optical data, with the mode in the ice observations occurring about 0.5 K below the frost point. We found that CALIOP PSCs identified as liquid/NAT mixtures exhibit two distinct preferred modes. One mode is significantly out of thermodynamic equilibrium with respect to NAT (4–5 K below the equilibrium NAT existence temperature), with HNO_3 uptake dominated by the more numerous liquid droplets. The other liquid/NAT mixture mode is much closer to NAT thermodynamic equilibrium, indicating that the particles have been exposed to temperatures below the NAT existence temperature for extended periods of time. The CALIOP PSC composition classification scheme was found to be excellent in an overall sense, and we have a good understanding of the cause of the minor misclassifications that do occur. We will investigate means to correct these deficiencies in our next generation algorithm.

ACPD

12, 24643–24676, 2012

1 Introduction

Polar stratospheric clouds (PSCs) play two essential roles in the springtime chemical depletion of ozone at high latitudes (Solomon, 1999). First of all, PSC particles serve as catalytic sites for heterogeneous chemical reactions that transform stable chlorine and bromine reservoir species into highly reactive ozone-destructive forms. These heterogeneous reactions are most efficient on liquid supercooled ternary ($HNO_3/H_2SO_4/H_2O$) solution (STS) PSC particles because of the larger total surface area and higher reaction efficiencies associated with STS (Lowe and MacKenzie, 2008). Secondly, if PSC particles grow sufficiently large, they can remove gaseous odd nitrogen from the lower stratosphere through gravitational sedimentation, which slows the reformation of the chlorine reservoirs and prolongs the ozone depletion process. This so-called denitrification is caused primarily by solid nitric acid trihydrate (NAT) PSC particles because the high number density ($\sim 10\,cm^{-3}$) of STS particles limits them to sub-micron sizes with concomitantly small fall speeds. Thus, it is important to better understand particle composition in order to capture PSCs processes more accurately in global models used to predict the future state of the stratospheric ozone layer.

Spaceborne observations from the CALIOP (Cloud-Aerosol Lidar with Orthogonal Polarization) lidar on the CALIPSO (Cloud-Aerosol Lidar and Infrared Pathfinder Satellite Observations) satellite, which commenced in June 2006, are providing a rich new dataset for studying PSCs (e.g., Noel et al., 2008; Pitts et al., 2007, 2009, 2011; Noel and Pitts, 2012). CALIPSO is part of the NASA A-train satellite constellation (Stephens et al., 2002), flying in formation with the Aqua, CloudSat, and Aura satellites. Pitts et al. (2009) (hereafter referred to as P09) developed an approach for both detection and composition classification of PSCs observed by CALIOP. The P09 composition classification algorithm infers PSC composition based on theoretical calculations of 532-nm backscatter and depolarization for non-equilibrium external mixtures of liquid (binary H_2SO_4/H_2O or STS) and solid NAT or ice particles, which ground-based and airborne

ACPD
12, 24643–24676, 2012

lidar measurements indicate are quite common (e.g., Biele et al., 2001; Toon et al., 2000).

In the absence of simultaneous in situ particle observations, the CALIOP PSC composition classification scheme can be evaluated by comparison with other remote measurements that provide information on particle composition. In one such study, Höpfner et al. (2009) reported a high degree of consistency between CALIOP PSC compositions for the 2006–2007 Antarctic and 2006/07–2007/08 Arctic winters and those derived from MIPAS (Michelson Interferometer for Passive Atmospheric Sounding) data on the Envisat spacecraft. A finding of particular note was that for PSCs in which the spectral signature of NAT was detected by MIPAS, about 90 % of coincident CALIOP data were classified as mixed liquid/NAT clouds, lending credence to the CALIOP composition classification scheme.

A recent study of the early 2008 Antarctic PSC season by Lambert et al. (2012) demonstrated that one can also gain valuable insight into PSC processes by analyzing the CALIOP data in combination with nearly coincident gas phase HNO_3 and H_2O measurements from the Microwave Limb Sounder (MLS) on the Aura satellite. Since HNO_3 and/or H_2O are the major constituents of all PSC particles (STS, NAT, and H_2O ice), tracking their uptake by PSCs as a function of temperature using MLS data provides constraints on particle composition and volume density. In this study, we follow the approach of Lambert et al. (2012) to analyze CALIOP PSC observations from 2006–2011 in conjunction with the Aura MLS data and temperature analyses from the Goddard Earth Observing System Data Assimilation System (GEOS-5 DAS). Comparison of the observed uptake of HNO_3 by CALIOP PSCs with modeled uptake for equilibrium STS and NAT indicates how well PSCs in the various composition classes conform to expected temperature existence regimes and offers some insight into the kinetics of PSC growth. The overarching goals of this paper are to assess the robustness of the P09 composition classification algorithm and identify potential improvements that can be implemented in the next generation algorithm.

ACPD
12, 24643–24676, 2012

2 Datasets

2.1 CALIOP PSC data

CALIOP was launched aboard the CALIPSO satellite in April 2006 and became operational in June 2006. CALIPSO is in a 98.2° inclination orbit which provides excellent coverage over the polar regions of both hemispheres with measurements up to about 82° latitude. CALIOP is a dual-wavelength (532 nm and 1064 nm), polarization-sensitive (532 nm) elastic backscatter lidar (Winker et al., 2009). The polarization sensitive measurements allow discrimination between spherical (liquid) and non-spherical (solid) particles. A more detailed description of CALIOP and its on-orbit performance can be found in Hunt et al. (2009) and information on calibration of the CALIOP data can be found in Powell et al. (2009).

The P09 PSC detection algorithm uses both the CALIOP 532-nm scattering ratio (R_{532}, the ratio of total to molecular backscatter, e.g., Cairo et al., 1999) and the 532-nm perpendicular backscatter coefficient (β_{perp}). A CALIOP observation is assumed to be a PSC if either R_{532} or β_{perp} exceeds a statistical threshold defined as the median plus four times the median deviation of the background aerosol ensemble (those data at temperatures above 200 K). The CALIOP data are initially smoothed to a common 5-km horizontal by 180-m vertical grid, and PSC detection is then performed using a successive horizontal averaging (5, 15, 45, 135 km) procedure. This ensures that optically thicker clouds (e.g., ice and fully developed STS) are detected at the finest possible spatial resolution while also enhancing the detection of tenuous PSCs (e.g., low number density NAT mixtures) that are detectable only through additional averaging. The P09 algorithm also introduced a scheme for classifying PSCs by composition based on comparison of CALIOP aerosol depolarization ratio (δ_{aerosol}, the ratio of the perpendicular to parallel components of aerosol backscatter, e.g., Cairo et al., 1999) and inverse scattering ratio ($1/R_{532}$) with theoretical optical calculations for equilibrium STS and representative non-equilibrium external liquid-solid particle mixtures, assuming 50 hPa atmospheric pressure and nominal mixing ratios of 10 ppbv HNO_3 and 5 ppmv H_2O. As

ACPD
12, 24643–24676, 2012

subsequently modified by Pitts et al. (2011) (hereafter referred to as P11), the CALIOP PSC algorithm now includes six composition classes: three classes of liquid/NAT mixtures, with Mix1, Mix2, and Mix2-enhanced denoting increasingly higher NAT number density/volume; STS (which also includes low number densities of NAT particles whose optical signature is masked by the much more numerous STS droplets at cold temperatures); H_2O ice; and mountain wave ice, the latter having high particle number densities ($\sim 10\,cm^{-3}$) but concomitantly small (1.0–1.5 µm radius) particles. Figure 1 shows a composite 2-D histogram of CALIOP PSC observations from the 2009–2010 Arctic winter in the $\delta_{aerosol}$ vs. $1/R_{532}$ coordinate system, with the boundaries of the six composition classes denoted by the black lines. The boundaries drawn between the composition classes are based on a limited set of optical calculations and, with the exception of the boundary separating STS from Mix1/Mix2/ice (P09), do not reflect the inherent uncertainty in the CALIOP measurements, especially in β_{perp}. Hence, the boundaries should be considered fuzzy, and "jumps" between adjacent composition classes occurring on small spatial scales may be simply a reflection of measurement noise rather than a true change in cloud composition.

For this study, we have made a slight modification to the P09/P11 composition classification scheme. PSC detection and composition classification were done independently in the P09/P11 algorithm and, as a result, it is possible that a PSC may be detected through an enhancement in β_{perp}, a clear indication of the presence of solid particles, but the derived $\delta_{aerosol}$ may fall into the STS composition regime due to noise in the calculated aerosol depolarization ratio. Similarly, a cloud may be detected strictly through an enhancement in R_{532} (no detectable enhancement in β_{perp}), yet the derived $\delta_{aerosol}$ may fall into one of the mixture regimes. Although this discrepancy only impacts a very small fraction of PSC observations, it is straightforward to correct by including two additional constraints to the P09/P11 composition classification scheme: (1) if a PSC is detected through an enhancement in β_{perp}, it will be classified as a liquid/NAT mixture or ice PSC (depending on the magnitude of R_{532}) regardless of its derived $\delta_{aerosol}$ value (similar to the constraint imposed by Lambert et al., 2012), and (2) if a

ACPD
12, 24643–24676, 2012

PSC does not exhibit an enhancement in β_{perp}, it will be classified as STS regardless of its derived $\delta_{aerosol}$ value.

Temperature profiles at each CALIOP measurement location are also included in the CALIOP Level 1 data files. The temperature data have been interpolated to the CALIOP Level 1 measurement locations from the Goddard Earth Observing System Model, Version 5 (GEOS-5) six-hourly gridded analyses (Rienecker et al., 2008). To match the standard PSC grid, the GEOS-5 data are smoothed to the 5-km horizontal resolution and interpolated to the 180-m vertical grid.

2.2 Aura MLS

The Aura MLS detects thermal microwave emission from the Earth's limb (Waters et al., 2006) along the line-of-sight in the forward direction of the Aura spacecraft flight track. Vertical scans made from the Earth's surface to a 90 km tangent height every 24.7 s provide a total of 3500 vertical profiles per day with a horizontal along track spacing of 1.5 degrees (165 km) and nearly global latitude coverage from 82° S–82° N. The limb radiance measurements are inverted using a 2-D optimal estimation retrieval (Livesey et al., 2006) to yield atmospheric profiles of temperature and composition in the vertical range 8–90 km (Livesey et al., 2006). The MLS version 3.3 measurements (Livesey et al., 2011) have typical single-profile precisions of 4–15 % for H_2O (Read et al., 2007; Lambert et al., 2007) and 0.7 ppbv for HNO_3 (Santee et al., 2007). Vertical and horizontal along-track resolutions are 3.1–3.5 km and 180–290 km for H_2O, and 3.5–5.5 km and 400–550 km for HNO_3.

Since Aura flies in formation with CALIPSO in the A-train satellite constellation, CALIOP and MLS measurement tracks are closely aligned with spatial and temporal differences less than 10 km and 30 s after a repositioning of the Aura satellite in 2008 and about 200 km and 7–8 min. prior to 2008 (see Lambert et al., 2012). To produce a co-located dataset, the MLS gas species measurements are interpolated to the CALIOP PSC grid using a weighted average of the two nearest MLS profiles. In addition, ancillary meteorological parameters from the Aura MLS Derived

ACPD
12, 24643–24676, 2012

Meteorological Products (DMPs), such as equivalent latitude, are also mapped onto the PSC grid.

3 Data analyses

Our basic approach is to combine CALIOP PSC observations with nearly coincident Aura MLS gas species measurements and GEOS-5 temperature analyses to track the uptake of gas phase HNO_3 as a function of temperature. Comparing the observed HNO_3 uptake with theoretical equilibrium HNO_3 uptake for NAT and STS indicates how well CALIOP PSCs in the various composition classes conform to expected temperature existence regimes and also offers some insight into PSC growth kinetics. Figure 2 shows theoretical gas-phase HNO_3 uptake curves assuming thermodynamic equilibrium conditions for STS (Carslaw et al., 1995) and NAT (Hanson and Mauersberger, 1988) at pressures of 30 and 50 hPa, assuming mixing ratios of 5 and 10 ppbv of total HNO_3, 5 ppmv of H_2O, and 0.1 ppbv H_2SO_4. The curves are presented as a function of absolute temperature in Fig. 2a and as a function of $T - T_{ice}$ in Fig. 2b, where T_{ice} is the frost point temperature calculated using the Murphy and Koop (2005) relationship. The figure illustrates clearly that in the $T - T_{ice}$ coordinate system, the individual curves collapse into essentially single STS and NAT uptake curves, removing variations due to differences in atmospheric pressure level and local changes in H_2O partial pressure (Drdla et al., 2003).

For this assessment, we examined the CALIOP PSC data record from both polar regions over the period from 2006 through 2011 and over a range of potential temperature levels spanning the 15–30 km altitude range. As will be discussed in Sect. 4, particle sedimentation and subsequent denitrification complicate the interpretation of the gas-phase HNO_3 uptake and can also affect composition classification. As a result, data from the Antarctic, where the stratosphere is subject to severe denitrification and partial dehydration every winter, are particularly difficult to interpret. For discussion, we focus on CALIOP and MLS data from the 2009–2010 Arctic winter which

ACPD
12, 24643–24676, 2012

complemented focused measurements from an extensive field campaign under the European Union RECONCILE (reconciliation of essential process parameters for an enhanced predictability of Arctic stratospheric ozone loss and its climate interactions) project conducted that winter from Kiruna, Sweden (P11; Dörnbrack et al., 2012). The 2009–2010 winter was characterized by unusually cold conditions in the stratosphere from mid-December through January that resulted in widespread PSCs (Dörnbrack et al., 2012; P11, Khosrawi et al., 2011). The distribution of PSCs observed by CALIOP during the 2009–2010 winter (Fig. 1) spans nearly the entire δ_{aerosol} vs. $1/R_{532}$ measurement space with significant numbers of PSCs in all six composition classes, providing an excellent dataset for assessing the robustness of our composition classification. Although denitrification occurred during the 2009–2010 Arctic winter, average HNO_3 abundances between 475–575 K potential temperature in January were close to 10 ppbv (Khosrawi et al., 2011), our standard value for defining the composition boundaries. We will examine an Antarctic case later in the paper to illustrate how severe denitrification/dehydration impacts our composition classification.

An interesting aspect of the 2009–2010 winter was the observation by CALIOP of tenuous liquid/NAT mixture PSCs with low NAT number densities in December, prior to the occurrence of ice (P11). These observations support the conclusions of Voigt et al. (2005) and Pagan et al. (2004) that ice nuclei are not a prerequisite for NAT PSC formation. To examine our classification scheme prior to the onset of denitrification, we will analyse this period (1–30 December 2009) separately. The remainder of the PSC season (31 December 2009–31 January 2010) was characterized by extensive regions of PSCs in all composition classes. 2-D histograms of CALIOP PSC observations for these two periods are shown in Fig. 3.

Figure 4 shows 2-D histograms of MLS HNO_3 uptake vs. $T - T_{\text{ice}}$ for CALIOP PSC observations by composition class for 1–30 December at the 490 K potential temperature level ($\sim$ 21 km). T is the ambient temperature at the CALIOP observation point (from the GEOS-5 gridded analyses) and T_{ice} is the frost point temperature (Murphy and Koop, 2005) calculated using the coincident Aura MLS gas-phase H_2O abundance. As

ACPD
12, 24643–24676, 2012

a guide for the reader's eye, reference equilibrium uptake curves for STS and NAT are overlaid in the figures assuming total abundances of 16 ppbv HNO_3 and 5 ppmv H_2O, which are representative of early season values at this level. As vortex temperatures fell below NAT equilibrium during mid-December, tenuous NAT mixture clouds were observed, with some indication of STS clouds on the coldest days. No ice or Mix2-enh PSCs were observed during this period. The majority of Mix1 and Mix2 PSC observations are in an uptake regime that falls between the reference NAT and STS equilibrium uptake curves at temperatures between $T_{ice} + 1$ K and $T_{ice} + 7$ K, with a larger range of HNO_3 uptake occurring on Mix2 particles. The observed uptake suggests that these non-equilibrium NAT mixtures have been exposed to temperatures below T_{NAT} for moderate time periods, but not long enough for the NAT particles to reach thermodynamic equilibrium. The limited number of STS observations during this period is not sufficient to adequately assess this composition class at this time.

Histograms of HNO_3 uptake as a function of $T - T_{ice}$ for 31 December–31 January are shown in Fig. 5. PSCs in all composition classes were observed during this period. Most observations in the STS class (Fig. 5a) are clearly aligned with the reference STS equilibrium uptake curve, as would be anticipated since STS particles are thought to grow fast enough to maintain equilibrium with the gas phase HNO_3. The main STS data cluster does lie at slightly lower temperatures than the reference equilibrium curve, a finding consistent with Lambert et al. (2012). Also of note is the secondary family of STS observations that lie along the reference NAT equilibrium uptake curve at temperatures too warm to support STS existence. These points are classified as STS because they do not exhibit a detectable enhancement in perpendicular backscatter, which would signal the presence of solid particles. An example of points classified as STS but at anomalously warm temperatures is shown in Fig. 6 for a PSC observed by CALIOP along an orbit track on 9 January 2010. Although the vast majority of CALIOP observations in this PSC scene are classified as NAT mixtures, there is a speckling of STS points (green pixels) throughout the cloud. These points are also likely to be NAT mixtures, but are misclassified as STS due to negative noise excursions in their

ACPD
12, 24643–24676, 2012

observed perpendicular backscatter signal, which lowers the measured perpendicular backscatter to values below our detection threshold for NAT particles. Hereafter we refer to this noise-induced misclassification as "speckle" based on how it manifests itself in CALIOP PSC images. For the 2009–2010 winter, we estimate that approximately 6 % of all measurements classified as STS are likely NAT mixtures misclassified due to speckle. Similar noise-induced misclassification likely occurs to some degree in all composition classes, but is only detectable when the misclassification puts the composition in an unexpected temperature regime. It may be possible to eliminate speckle by applying a spatial filter that assumes composition homogeneity over appropriately small spatial scales. This will be investigated for our next generation algorithm.

The HNO_3 uptake as a function of $T - T_{ice}$ for PSCs identified as NAT mixtures by our composition classification scheme are shown in Fig. 5b–d. The mixture observations cover a broad range of temperatures from 7–8 K above the frost point to near the frost point. The uptake of HNO_3 for each of the mixture classes has two distinct modes: one closely aligned with the STS equilibrium curve and another aligned with the NAT equilibrium curve, but there are also numerous points falling in between the two reference curves. At first glance, the mixture points that exhibit HNO_3 uptake similar to STS may appear to be misclassified STS. However, these points actually represent STS/NAT mixtures in which the uptake of HNO_3 by the relatively low number density NAT particles is a slow process, whereas HNO_3 condensation on the much more numerous liquid droplets occurs rapidly in response to decreases in temperature. In these mixture cases, the presence of the NAT particles produces a detectable enhancement in the CALIOP perpendicular backscatter signal, hence their classification as NAT mixtures, but at colder temperatures the more numerous liquid droplets dominate the uptake of HNO_3. For these mixtures, the CALIOP perpendicular backscatter signal is more sensitive to the presence of the NAT particles than the MLS gas-phase HNO_3 uptake observations. The second mode of NAT mixture observations is more closely aligned with the NAT equilibrium uptake curve. For these cases, the NAT particles were likely exposed to temperatures below NAT equilibrium for extended periods

ACPD
12, 24643–24676, 2012

of time, allowing a larger fraction of the gas phase HNO_3 to condense onto the NAT particles and bringing the mixture closer to thermodynamic equilibrium.

The HNO_3 uptake for observations identified as ice PSCs during this period is shown in Fig. 5e. Ice PSCs are expected to occur only at temperatures below the frost point, with almost complete uptake of gas-phase HNO_3 by STS (or NAT) prior to the temperature having reached the frost point. In the CALIOP observations, there is a clear maximum in ice PSCs at temperatures near or below the frost point and HNO_3 values below 2 ppbv, but ice observations also extend to temperatures above the frost point and larger HNO_3 abundances. Although this would appear to be a misclassification, i.e. ice PSCs occurring at temperatures outside their expected thermodynamic existence regime, we are confident that the ice classification is correct since the large optical signal (both R_{532} and β_{perp}) produced by ice PSCs is a robust signature. The anomalous points in Fig. 5e are likely caused by differences in measurement resolution among CALIOP, GEOS-5, and MLS. During the first half of this period (31 December–14 January), the vast majority of ice PSCs were associated with orographic wave events that occurred on relatively small spatial scales (e.g., P11). With the high spatial resolution sampling of CALIOP and the inherently large scattering ratio values associated with ice PSCs, mountain wave ice PSCs are easily detected and properly classified by CALIOP at the highest PSC resolution (5 km × 180 m). However, given the relatively coarse resolution of both the GEOS-5 gridded analyses (0.5 degrees) and Aura MLS HNO_3 measurements (400–550 km horizontal × 3.5–5.5 km vertical), small scale wave features are more difficult to fully resolve. The amplitude of the temperature perturbations associated with these waves is typically underestimated in the GEOS-5 gridded analyses, and the localized uptake of HNO_3 by the STS in the cold phase of the waves will be underestimated by MLS. To illustrate this point further, gas-phase HNO_3 uptake associated with CALIOP ice PSCs for the two distinct periods are shown in Fig. 7. The ice observations at anomalously warm temperatures and relatively large HNO_3 mixing ratios are primarily confined to the first two weeks of January when mountain waves were the main forcing mechanism for ice cloud formation. After about 15 January, ice

ACPD
12, 24643–24676, 2012

PSCs were observed on much larger spatial scales associated with synoptic-scale regions of temperatures below the frost point, and both GEOS-5 and MLS are able to better resolve such features.

Histograms of PSC occurrence vs. $T - T_{ice}$ and $T - T_{eq}$ for 31 December 2009–31 January 2010 are depicted in Fig. 8 for all CALIOP composition classes shown in Fig. 5. T_{eq} is defined as T_{ice}, T_{NAT}, or T_{STS}, depending on the PSC composition classification, and is calculated using the Murphy and Koop (2005) (T_{ice}), Hanson and Mauersberger (1988) (T_{NAT}), and Carslaw et al. (1995) (T_{STS}) relationships with the coincident MLS HNO_3 and H_2O abundances. For compositions other than ice, the histograms are restricted to observations with HNO_3 values greater than 1 ppbv to avoid the region where the NAT and STS equilibrium curves converge. To a large degree, observations in each composition class conform to their expected temperature existence regimes, except for the points misclassified as STS at too warm temperatures (speckle) and the warm-biased ice PSCs associated with small-scale orographic waves. Ignoring the positive tail in the distribution of STS observations due to speckle, STS PSCs occur over a relative narrow temperature range centered about 1 K below the STS equilibrium temperature. The peak at 1 K below equilibrium may be an indication of a cold bias in the GEOS-5 temperature analyses as noted by Lambert et al. (2012). The distribution of each NAT mixture class has a bimodal appearance with one mode near the NAT equilibrium temperature and a second, more populous mode at 4-5 K below NAT equilibrium – which is very near the STS mode in $T - T_{ice}$ space (Fig. 8a). This more populous mode is far out of equilibrium with respect to NAT and corresponds to mixtures with NAT particles producing a large enough perpendicular backscatter signal to be detectable by CALIOP, but whose gas-phase HNO_3 uptake is dominated by the much more numerous STS droplets. The fact that the NAT mixture histograms are distinctly bimodal, i.e. the mixtures do not occur uniformly over the space between T_{NAT} and T_{STS}, is quite interesting and may indicate a rapid switch from the thermodynamically metastable STS to stable NAT after sufficient exposure of air parcels to temperatures below T_{NAT}. The mode of the ice PSC distribution is centered at a temperature slightly below the

ACPD
12, 24643–24676, 2012

frost point (also consistent with Lambert et al., 2012) with a full-width-half-maximum of about 1.5 K. The longer positive tail in the ice PSC distribution is due to warm biased temperatures associated with the wave ice events.

Histograms of PSC occurrence vs. $T - T_{ice}$ and $T - T_{eq}$ for five seasons in the Arctic (2006–2011) are shown in Fig. 9. These multi-year histograms are similar in nature to as those for the 2009–10 Arctic season (Fig. 8), with observations in all composition classes conforming to expected thermodynamic existence regimes. The notable exceptions again are observations classified as STS at anomalously warm temperatures, which are likely NAT clouds misclassified due to noise in β_{perp} (speckle) and the ice PSCs at (apparent) temperatures above the frost point, which are associated with orographic waves, the predominant mechanism for ice PSC formation in the Arctic. Composition classification is also robust in the Antarctic, as illustrated by the histograms of PSC occurrence vs. $T - T_{ice}$ and $T - T_{eq}$ for six seasons in the Antarctic (2006–2011) in Fig. 10. Although less pronounced in than in the Arctic, a small number of anomalously warm STS points also appear in the Antarctic STS histogram. Ice PSC formation in the Antarctic occurs more frequently and generally on larger spatial scales than in the Arctic and as a consequence the number of ice PSCs at (apparent) temperatures above the frost point are less common. These multi-year histograms represent over 1.7 million Arctic and 10.1 million Antarctic PSC observations and provide compelling evidence that the P09/P11 composition classification is robust.

4 Impact of denitrification on composition classification

The composition class boundaries defined by P09 and P11 are based on a standard set of conditions: 50 hPa atmospheric pressure and nominal mixing ratios of 10 ppbv HNO_3 and 5 ppmv H_2O. For most Arctic winters and early in the Antarctic winter, these values are representative. However, the Antarctic is subject to severe denitrification and partial dehydration every winter, with HNO_3 being nearly totally depleted at times in the interior of the vortex. These extreme conditions can have a significant impact

ACPD
12, 24643–24676, 2012

on the composition class boundaries. Shown in Fig. 11a are theoretical calculations of CALIOP optical signals for various liquid/NAT mixtures and ice computed for the standard conditions (10 ppbv HNO_3). The ice PSCs are the arm of points extending up and to the right from the STS domain at $1/R_{532} \sim 0.2$. For comparison, Fig. 11b depicts theoretical calculations for denitrified conditions of 5 ppbv HNO_3. The reduction in available condensable HNO_3 limits the growth potential of the particles, resulting in a systematic shift of the optical signals to smaller scattering ratios (larger $1/R_{532}$) values. For these conditions, the arm of ice points is shifted to the left and departs from the STS domain at $1/R_{532} \sim 0.3$. Therefore, to properly account for denitrification in our composition classification scheme, the boundary between ice and NAT mixture (Mix2 and Mix2-enh) PSC domains should shifted to smaller scattering ratio values (larger $1/R_{532}$ values). The magnitude of the shift is a function of the total abundance of HNO_3.

The effects of denitrification can also clearly be seen in the CALIOP PSC observations. For example, shown in Fig. 12a is the distribution of PSCs observed by CALIOP for June 2009 in an equivalent latitude band between 60° S and 70° S. The total HNO_3 mixing ratio during June was decreasing as denitrification began, but on average was close to our standard value of 10 ppbv. The period was dominated by fully developed STS (maximum along the $\delta_{aerosol} = 0$ axis) and ice PSCs, with a small number of mixtures. Similar to the theoretical calculations (Fig. 11a), the arm of ice PSC observations (dashed white line) departs from the STS maximum at $1/R_{532}$ values of 0.2. In contrast, Fig. 12b depicts CALIOP observations in August 2009 deep inside the vortex at equivalent latitudes between 75° S and 90° S. The total HNO_3 abundance at this time had dropped significantly from early season values to around 5 ppbv or less resulting in a discernible shift in the point where the axis of the ice arm departs from the STS mode, to a $1/R_{532}$ value of about 0.3 (similar to Fig. 11b).

The implication from Figs. 11 and 12 is that some ice PSCs are being misclassified as NAT mixtures during periods of moderate to severe denitrification, which primarily occur in the Antarctic. To explore this possibility in more detail, we examine ice and

ACPD
12, 24643–24676, 2012

Mix2 PSC observations from the Antarctic during August 2009, when denitrification is severe. Histograms of ice and Mix2-enh PSC occurrence as a function of $T - T_{ice}$ from the interior of the vortex in August 2009 are shown in Fig. 13. Figure 13a depicts histograms for composition classification using our standard ice/Mix2-enh boundary ($1/R_{532} = 0.2$). With random measurement noise and no bias in temperature and T_{ice}, one would expect the ice PSC histogram to be Gaussian with a mode at $T - T_{ice} = 0$. The mode of the actual histogram is slightly below the frost point, but the positive tail of the distribution appears to be truncated relative to the negative tail. The Mix2-enh distribution also has a maximum near the frost point, some of which may be misclassified ice, but also extends to warmer temperatures as would be expected for NAT mixtures. To account for denitrification in our composition classification, we should shift the composition boundaries appropriately based on the total abundance of HNO_3. To demonstrate this, Fig. 13b shows histograms for composition classification using an ice/mix2-enh boundary of $1/R_{532} = 0.3$. For this case, there has been a redistribution of compositions with over a 50 % increase in the number of ice clouds which had been classified as Mix2-enh in our standard case. The shape of the ice PSC distribution in this case appears to be more Gaussian-like than in the standard case, with no obvious truncation of the positive tail. Figure 13c shows histograms for composition classification using an ice/mix2-enh boundary of $1/R_{532} = 0.4$. This results in more than a doubling of the number of ice PSCs relative to the standard case, but the ice PSC distribution now shows a noticeable extension to warmer temperatures ($T_{ice} + 3$ K), indicating that the boundary has been shifted too far to the left and with some Mix2-enh clouds now being misclassified as ice. In practice, it will be difficult to accurately account for the magnitude of denitrification since most HNO_3 measurements are gas phase only and are impacted by uptake on PSC particles.

ACPD
12, 24643–24676, 2012

5 Summary and future direction

We have used Aura MLS gas phase HNO_3 and H_2O measurements along with GEOS-5 temperature analyses to independently assess the CALIOP PSC composition classification scheme, which is based solely on the lidar optical measurements. Our approach was to examine the uptake of HNO_3 as a function of $T - T_{ice}$ to determine if the assigned PSC composition is consistent with the thermodynamic existence regimes for STS, NAT, and ice. The results indicate that, overall, the CALIOP PSC composition classification performance is excellent with each class exhibiting uptake behavior consistent with theoretical expectations.

PSCs identified as STS exhibit gas phase uptake of HNO_3 consistent with theory, but with a small temperature bias, consistent with previous studies. Some ($\sim$6 %) of points being classified as STS are actually liquid/NAT mixtures being misclassified due to the so-called speckle effect caused by pixel-scale negative noise excursions in the CALIOP perpendicular backscatter measurements. Although not detectable in these analyses, misclassification due to such speckle likely occurs at a similar rate in other composition classes.

PSCs identified as liquid/NAT mixtures exhibit two distinct preferred modes. One such mode is significantly out of thermodynamic equilibrium with respect to NAT (4–5 K below T_{NAT}), with HNO_3 uptake dominated by the more numerous liquid droplets. The other liquid/NAT mode is much closer to NAT thermodynamic equilibrium indicating that the particles have been exposed to temperatures below T_{NAT} for extended periods of time.

Ice PSC classification is robust in the CALIOP optical data, and the mode in the ice observations occurs about 0.5 K below the frost point. The anomalously warm temperatures and high HNO_3 values associated with CALIOP observations of small-scale ice clouds, such as orographic wave clouds, are due to the difficulty in resolving such features in the GEOS-5 and MLS data.

ACPD
12, 24643–24676, 2012

We also demonstrated that severe denitrification can impact the CALIOP composition classification. The P09/P11 composition class boundaries are based on nominal vapor abundances, and during periods of severe denitrification these boundaries should be adjusted to account for the reduced growth potential of the PSC particles. The biggest impact is a shift in the boundary between ice PSCs and NAT mixtures. As a result, some ice PSCs are being misclassified as NAT mixtures using the P09/P11 scheme during periods of moderate to severe denitrification, primarily in the Antarctic.

We will investigate methods to correct these deficiencies for our next generation algorithm.

Acknowledgements. The Aura MLS gas species data and Derived Meteorological Products (DMP) were provided courtesy of the MLS team and obtained through the Aura MLS website (http://mls.jpl.nasa.gov/index-eos-mls.php). We would also like to thank David Considine, Program Scientist for the CALIPSO/CloudSat Missions for continued support of this research. Support for L. Poole is provided under NASA contract NNL11AA10D. Work at the Jet Propulsion Laboratory, California Institute of Technology, was carried out under a contract with the National Aeronautics and Space Administration.

References

Biele, J., Tsias, A., Luo, B. P., Carslaw, K. S., Neuber, R., Beyerle, G., and Peter, T.: Nonequilibrium coexistence of solid and liquid particles in Arctic stratospheric clouds, J. Geophys. Res., 106, 22991–23007, 2001.

Cairo, F., Di Donfrancesco, G., Adriani, A., Pulvirenti, L., and Fierli, F.: Comparison of various linear depolarization parameters measured by lidar, Appl. Opt., 38, 4425–4432, 1999.

Carslaw, K. S., Luo, B. P., and Peter, T.: An analytic expression for the composition of aqueous HNO_3-H_2SO_4 stratospheric aerosols including gas phase removal of HNO_3, Geophys. Res. Lett., 22, 1877–1880, 1995.

Hanson, D. R. and Mauersberger, K.: Laboratory studies of the nitric acid trihydrate: Implications for the south polar stratosphere, Geophys. Res. Lett., 15, 855–858, 1988.

ACPD

12, 24643–24676, 2012

Höpfner, M., Pitts, M. C., and Poole, L. R.: Comparison between CALIPSO and MIPAS observations of polar stratospheric clouds, J. Geophys. Res., 114, D00H05, doi:10.1029/2009JD012114, 2009.

Hunt, W. H., Winker, D. M., Vaughan, M. A., Powell, K. A., Lucker, P. L., and Weimer, C.: CALIPSO Lidar Description and Performance Assessment, J. Atmos. Oceanic Technol., 26, 1214–1228, doi:10.1175/2009JTECHA1223.1, 2009.

Khosrawi, F., Urban, J., Pitts, M. C., Voelger, P., Achtert, P., Kaphlanov, M., Santee, M. L., Manney, G. L., Murtagh, D., and Fricke, K.-H.: Denitrification and polar stratospheric cloud formation during the Arctic winter 2009/2010, Atmos. Chem. Phys., 11, 8471–8487, doi:10.5194/acp-11-8471-2011, 2011.

Lambert, A., Read, W. G., Livesey, N. J., Santee, M. L., Manney, G. L., Froidevaux, L., Wu, D. L., Schwartz, M. J., Pumphrey, H. C., Jimenez, C., Nedoluha, G. E., Cofield, R. E., Cuddy, D. T., Daffer, W. H., Drouin, B. J., Fuller, R. A., Jarnot, R. F., Knosp, B. W., Pickett, H. M., Perun, V. S., Snyder, W. V., Stek, P. C., Thurstans, R. P., Wagner, P. A., Waters, J. W., Jucks, K. W., Toon, G. C., Stachnik, R. A., Bernath, P. F., Boone, C. D., Walker, K. A., Urban, J., Murtagh, D., Elkins, J. W., and Atlas, E.: Validation of the Aura Microwave Limb Sounder middle atmosphere water vapor and nitrous oxide measurements, J. Geophys. Res., 112, D24S36, doi:10.1029/2007JD008724, 2007.

Lambert, A., Santee, M. L., Wu, D. L., and Chae, J. H.: A-train CALIOP and MLS observations of early winter Antarctic polar stratospheric clouds and nitric acid in 2008, Atmos. Chem. Phys., 12, 2899–2931, doi:10.5194/acp-12-2899-2012, 2012.

Livesey, N. J., Snyder, W. V., Read, W. G., and Wagner, P. A.: Retrieval algorithms for the EOS Microwave Limb Sounder (MLS), IEEE T. Geosci. Remote, 44, 1144–1155, 2006.

Livesey, N. J., Read, W. G., Froidevaux, L., Lambert, A., Manney, G. L., Pumphrey, H. C., Santee, M. L., Schwartz, M. J., Wang, S., Cofield, R. E., Cuddy, D. T., Fuller, R. A., Jarnot, R. F., Jiang, J. H., Knosp, B. W., Stek, P. C., Wagner, P. A., and Wu, D. L.: Version 3.3 Level 3 data quality and description document, Tech. Rep. JPL D-33509, Jet Propulsion Laboratory, available at: http://mls.jpl.nasa.gov (last access: October 2011), 2011.

Lowe, D. and A. R. MacKenzie, Polar stratospheric cloud microphysics and chemistry, J. Atmos. Solar-Terr. Phys., 70, 13–40, 2008.

Murphy, D. M. and Koop, T. , Review of the vapour pressures of ice and supercooled water for atmospheric applications, Q. J. Roy. Meteorol. Soc., 131, 1539–1565, doi:10.1256/qj.04.94, 2005.

ACPD
12, 24643–24676, 2012

Noel, V. and Pitts, M.: Gravity wave events from mesoscale simulations compared to polar stratospheric clouds observed from spaceborne lidar over the Antarctic Peninsula, J. Geophys. Res., 117, D11207, doi:10.1029/2011JD017318, 2012.

Noel, V., Hertzog, A., Chepfer, H., and Winker, D., Polar stratospheric clouds over Antarctica from the CALIPSO spaceborne lidar, J. Geophys. Res., 113, D02205, doi:10.1029/2007JD008616, 2008.

Pagan, K. L., Tabazadeh, A., Drdla, K., Hervig, M. E., Eckermann, S. D., Browell, E. V., Legg, M. J., and Foschi, P. G.: Observational evidence against mountain-wave generation of ice nuclei as a prerequisite for the formation of three solid nitric acid polar stratospheric clouds observed in the Arctic in early December 1999, J. Geophys. Res., 109, D04312, doi:1029/2003JD003846, 2004.

Pitts, M. C., Thomason, L. W., Poole, L. R., and Winker, D. M.: Characterization of Polar Stratospheric Clouds with spaceborne lidar: CALIPSO and the 2006 Antarctic season, Atmos. Chem. Phys., 7, 5207–5228, doi:10.5194/acp-7-5207-2007, 2007.

Pitts, M. C., Poole, L. R., and Thomason, L. W.: CALIPSO polar stratospheric cloud observations: second-generation detection algorithm and composition discrimination, Atmos. Chem. Phys., 9, 7577–7589, doi:10.5194/acp-9-7577-2009, 2009.

Pitts, M. C., Poole, L. R., Dörnbrack, A., and Thomason, L. W.: The 2009–2010 Arctic polar stratospheric cloud season: a CALIPSO perspective, Atmos. Chem. Phys., 11, 2161–2177, doi:10.5194/acp-11-2161-2011, 2011.

Powell, K. A., Hostetler, C. A., Liu, Z., Vaughan, M. A., Kuehn, R. E., Hunt, W. H., Lee, K., Trepte, C. R., Rogers, R. R., Young, S. A., and Winker, D. M.: CALIPSO Lidar Calibration Algorithms: Part I – Nighttime 532 nm Parallel Channel and 532 nm Perpendicular Channel, J. Atmos. Oceanic Technol., 26, 2015–2033, doi:10.1175/2009JTECHA1242.1, 2009.

Read, W. G., Lambert, A., Bacmeister, J., Cofield, R. E., Christensen, L. E., Cuddy, D. T., Daffer, W. H., Drouin, B. J., Fetzer, E., Froidevaux, L., Fuller, R., Herman, R., Jarnot, R. F., Jiang, J. H., Jiang, Y. B., Kelly, K., Knosp, B. W., Kovalenko, L. J., Livesey, N. J., Liu, H. C., Manney, G. L., Pickett, H. M., Pumphrey, H. C., Rosenlof, K. H., Sabounchi, X., Santee, M. L., Schwartz, M. J., Snyder,W. V., Stek, P. C., Su, H., Takacs, L. L., Thurstans, R. P., Vomel, H., Wagner, P. A., Waters, J.W.,Webster, C. R.,Weinstock, E. M., and Wu, D. L.: Aura Microwave Limb Sounder upper tropospheric and lower stratospheric H_2O and relative humidity with respect to ice validation, J. Geophys. Res., 112, D24S35, doi:10.1029/2007JD008752, 2007.

ACPD

12, 24643–24676, 2012

Santee, M. L., Lambert, A., Read, W. G., Livesey, N. J., Cofield, R. E., Cuddy, D. T., Daffer, W. H., Drouin, B. J., Froidevaux, L., Fuller, R. A., Jarnot, R. F., Knosp, B. W., Manney, G. L., Perun, V. S., Snyder, W. V., Stek, P. C., Thurstans, R. P., Wagner, P. A., Waters, J. W., Muscari, G., de Zafra, R. L., Dibb, J. E., Fahey, D.W., Popp, P. J., Marcy, T. P., Jucks, K. W., Toon, G. C., Stachnik, R. A., Bernath, P. F., Boone, C. D., Walker, K. A., Urban, J., and Murtagh, D.: Validation of the Aura Microwave Limb Sounder HNO_3 measurements, J. Geophys. Res., 112, D24S40, doi:10.1029/2007JD008721, 2007.

Solomon, S.: Stratospheric ozone depletion: A review of concepts and history, Rev. Geophys., 37, 275–316, 1999.

Stephens, G. L., Vane, D. G., Boain, R. J., Mace, G. G., Sassen, K., Wang, Z., Illingworth, A. J., O'Connor, E. J., Rossow, W. B., Durden, S. L., Miller, S. D., Austin, R. T., Benedetti, A., Mitrescu, C., and the CloudSat Science Team: The CloudSat mission and the A-Train: A new dimension of space-based observations of clouds and precipitation, B. Am. Meteorol. Soc., 83, 1771–1790, 2002.

Toon, O., Tabazadeh, A., Browell, E., and Jordan, J.: Analysis of lidar observations of Arctic polar stratospheric clouds during January 1989, J. Geophys. Res., 105, 20589–20615, 2000.

Voigt, C., Schlager, H., Luo, B. P., Dörnbrack, A., Roiger, A., Stock, P., Curtius, J., Vössing, H., Borrmann, S., Davies, S., Konopka, P., Schiller, C., Shur, G., and Peter, T.: Nitric Acid Trihydrate (NAT) formation at low NAT supersaturation in Polar Stratospheric Clouds (PSCs), Atmos. Chem. Phys., 5, 1371–1380, doi:10.5194/acp-5-1371-2005, 2005

Waters, J. W., Froidevaux, L., Harwood, R. S., Jarnot, R. F., Pickett, H. M., Read, W. G., Siegel, P. H., Cofield, R. E., Filipiak, M. J., Flower, D. A., Holden, J. R., Lau, G. K. K., Livesey, N. J., Manney, G. L., Pumphrey, H. C., Santee, M. L., Wu, D. L., Cuddy, D. T., Lay, R. R., Loo, M. S., Perun, V. S., Schwartz, M. J., Stek, P. C., Thurstans, R. P., Boyles, M. A., Chandra, K. M., Chavez, M. C., Chen, G. S., Chudasama, B. V., Dodge, R., Fuller, R. A., Girard, M. A., Jiang, J. H., Jiang, Y. B., Oswald, J. E., Patel, N. C., Pukala, D. M., Quintero, O., Scaff, D., Van Snyder, W., Tope, M. C., Wagner, P. A., and Walch, M. J.: The Earth Observing System Microwave Limb Sounder (EOS MLS) on the Aura satellite, IEEE T. Geosci. Remote, 44, 1075–1092, 2006.

Winker, D. M., Vaughan, M. A., Omar, A. H., Hu, Y., Powell, K. A., Liu, Z., Hunt, W. H., and Young, S. A.: Overview of the CALIPSO Mission and CALIOP Data Processing Algorithms, J. Atmos. Oceanic Technol., 26, 2310–2323, doi:10.1175/2009JTECHA1281.1, 2009.

ACPD
12, 24643–24676, 2012

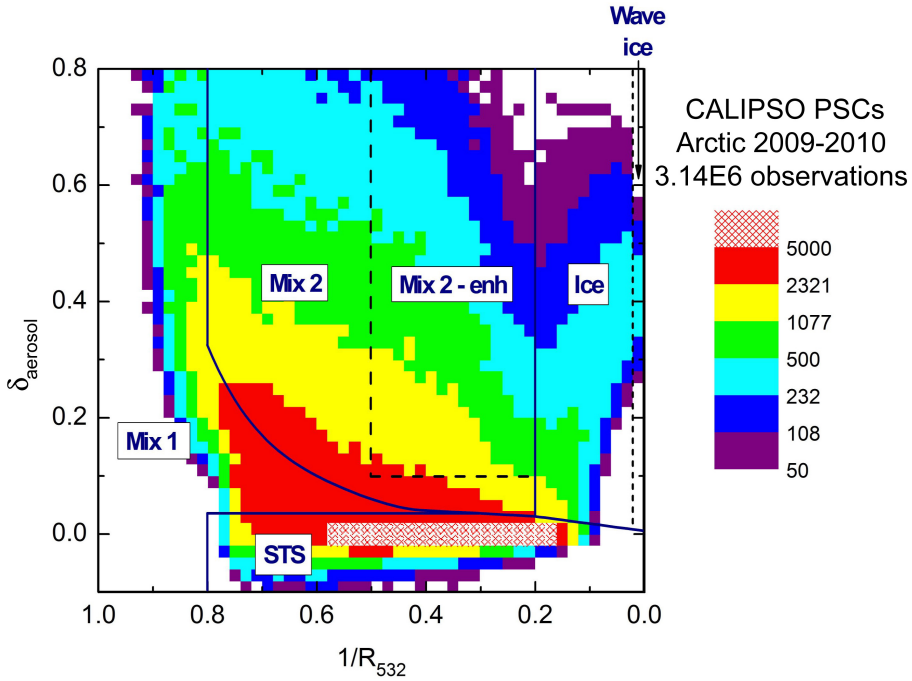

Fig. 1. Composite 2-D histogram of all CALIOP PSC observations during the 2009–2010 Arctic winter in the δ_{aerosol} vs. $1/R_{532}$ coordinate system, with the solid black lines denoting the boundaries of the six PSC composition domains defined by P09 and the dashed boxes denoting the domains of the two new composition sub-classes defined by P11. The histogram bin size is 0.02×0.02 (both unitless) and the color scale indicates the number of cloud observations falling within each bin.

ACPD
12, 24643–24676, 2012

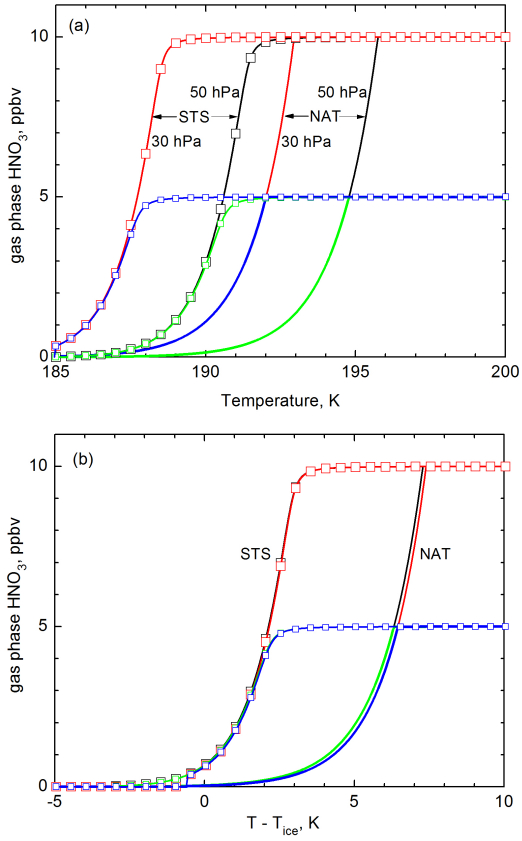

Fig. 2. Theoretical equilibrium uptake of HNO_3 by STS (square symbols) and NAT as a function of **(a)** temperature and **(b)** $T - T_{ice}$. Red and black curves/symbols: 10 ppbv HNO_3, 5 ppmv H_2O; blue and green curves/symbols: 5 ppbv HNO_3, 5 ppmv H_2O.

ACPD
12, 24643–24676, 2012

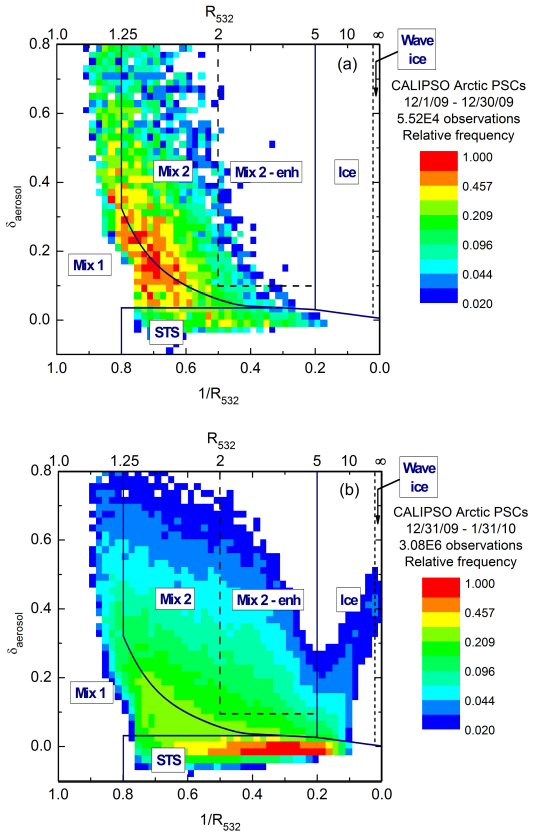

Fig. 3. Composite 2-D histogram of all CALIOP PSC observations for two periods of the 2009–2010 Arctic winter over the altitude range from 15–30 km in the δ_{aerosol} vs. $1/R_{532}$ coordinate system. Panel **(a)** represents the period from 1–30 December 2009 and Panel **(b)** represents the period from 31 December 2009–31 January 2010.

ACPD
12, 24643–24676, 2012

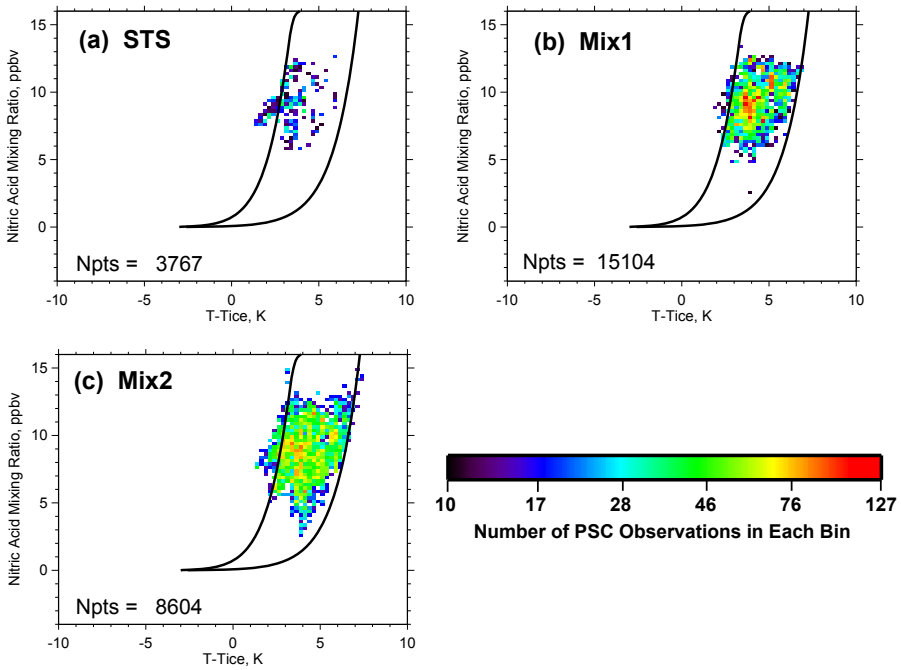

Fig. 4. Uptake of nitric acid as a function of $T - T_{ice}$ for CALIOP Arctic PSC observations at 490 K potential temperature during 1–30 December 2009 for **(a)** STS, **(b)** Mix1, and **(c)** Mix2 clouds. The histogram bin size is 0.25 ppbv × 0.25 K and the color scale indicates the number of cloud observations falling within each bin. Black lines are reference equilibrium uptake curves for STS (left) and NAT (right) assuming 16 ppbv HNO_3 and 5 ppbv H_2O.

ACPD
12, 24643–24676, 2012

CALIOP polar stratospheric cloud composition classification

M. C. Pitts et al.

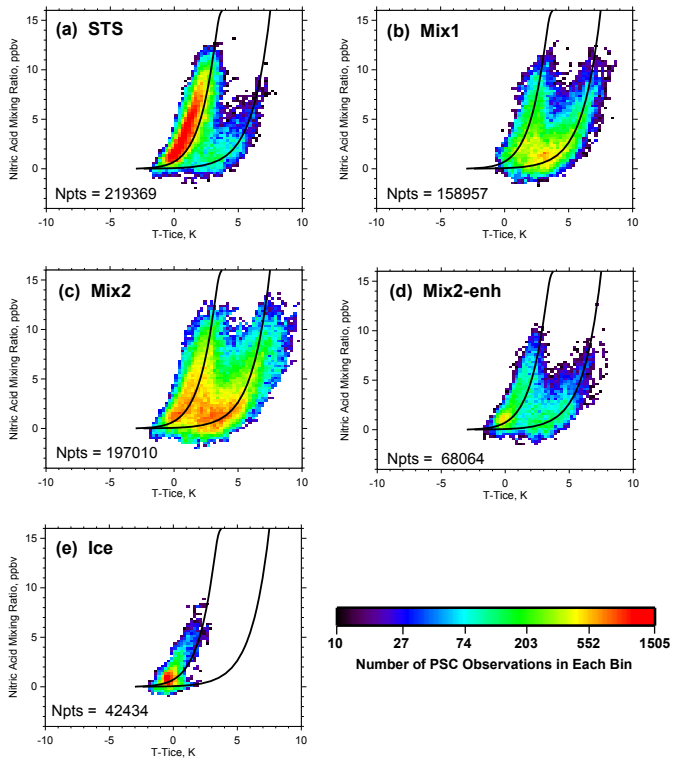

Fig. 5. Uptake of nitric acid as a function of $T - T_{ice}$ for CALIOP Arctic PSC observations at 490 K potential temperature during 31 December 2009–31 January 2010 for **(a)** STS, **(b)** Mix 1, **(c)** Mix 2, **(d)** Mix 2-enh, and **(e)** ice clouds. The histogram bin size is 0.25 ppbv × 0.25 K and the color scale indicates the number of cloud observations falling within each bin. Black lines are reference equilibrium uptake curves for STS (left) and NAT (right) assuming 16 ppbv HNO_3 and 5 ppbv H_2O.

ACPD
12, 24643–24676, 2012

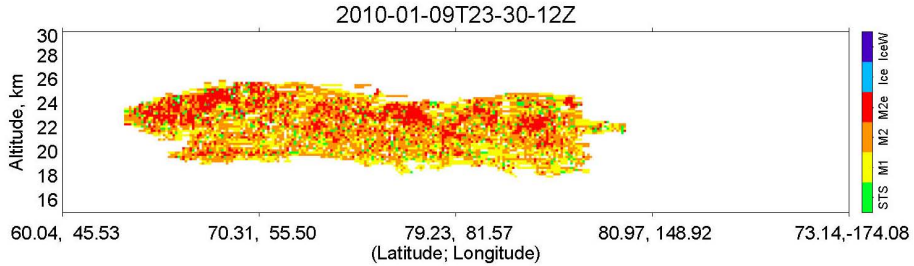

Fig. 6. Example of noise-induced misclassification in a CALIOP PSC scene from an orbit on 9 January 2010. PSC composition class is indicated by color scale at right.

ACPD
12, 24643–24676, 2012

CALIOP polar stratospheric cloud composition classification

M. C. Pitts et al.

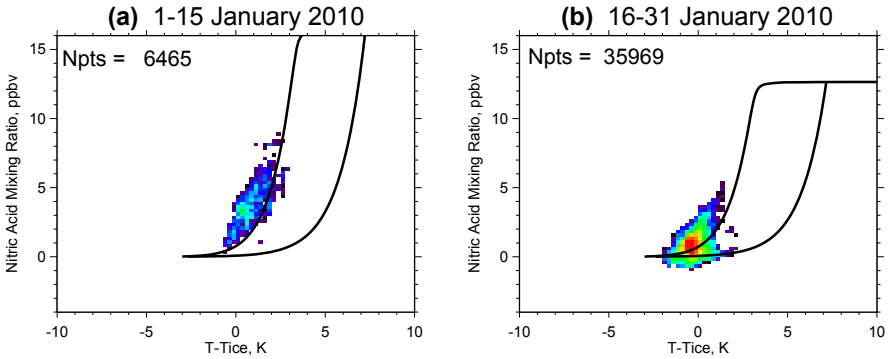

Fig. 7. HNO_3 uptake as a function of $T - T_{ice}$ for CALIOP ice PSC observations during **(a)** 1–15 January 2010 and **(b)** 16–31 January 2010. Orographic waves were the primary forcing mechanism for ice PSCs during 1–15 January, while larger-scale synoptic cooling formed ice PSCs during 16–31 January. The color scale is the same as in Fig. 5.

ACPD
12, 24643–24676, 2012

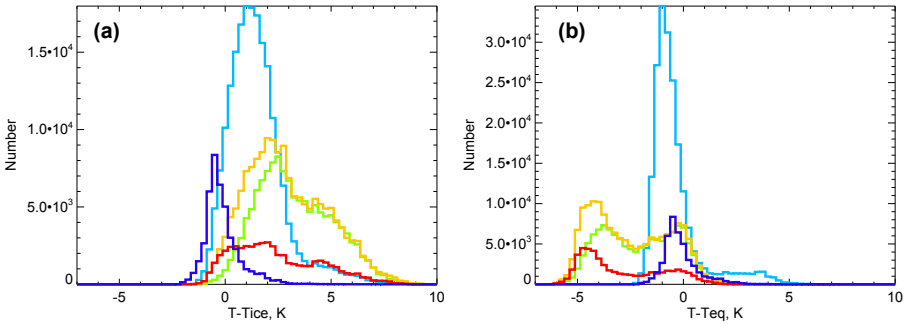

Fig. 8. Histograms of CALIOP PSC observations at 490 K potential temperature during 31 December 2009–31 January 2010 as a function of **(a)** $T - T_{ice}$ and **(b)** $T - T_{eq}$ by composition: STS (light blue), Mix1 (green), Mix2 (orange), Mix2-enh (red), and ice (dark blue).

ACPD
12, 24643–24676, 2012

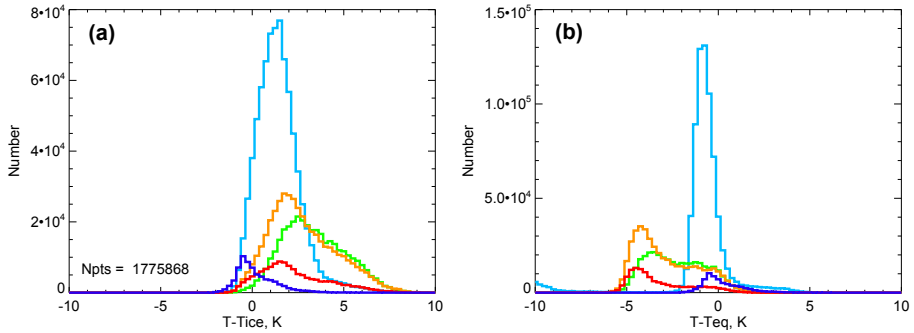

Fig. 9. Histograms of CALIOP PSC observations at 490 K potential temperature during five Arctic winters (2006–2011) as a function of **(a)** $T - T_{ice}$ and **(b)** $T - T_{eq}$ by composition: STS (light blue), Mix1 (green), Mix2 (orange), Mix2-enh (red), and ice (dark blue).

ACPD
12, 24643–24676, 2012

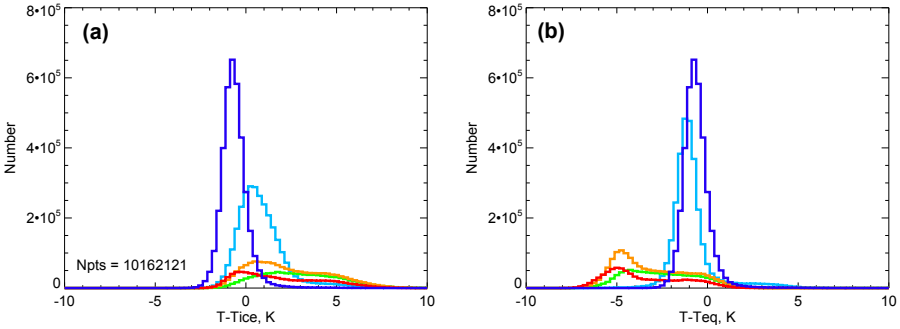

Fig. 10. Histograms of CALIOP PSC observations at 490 K potential temperature from six seasons in the Antarctic (2006–2011) as a function of **(a)** $T - T_{ice}$ and **(b)** $T - T_{eq}$ by composition: STS (light blue), Mix1 (green), Mix2 (orange), Mix2-enh (red), and ice (dark blue).

ACPD
12, 24643–24676, 2012

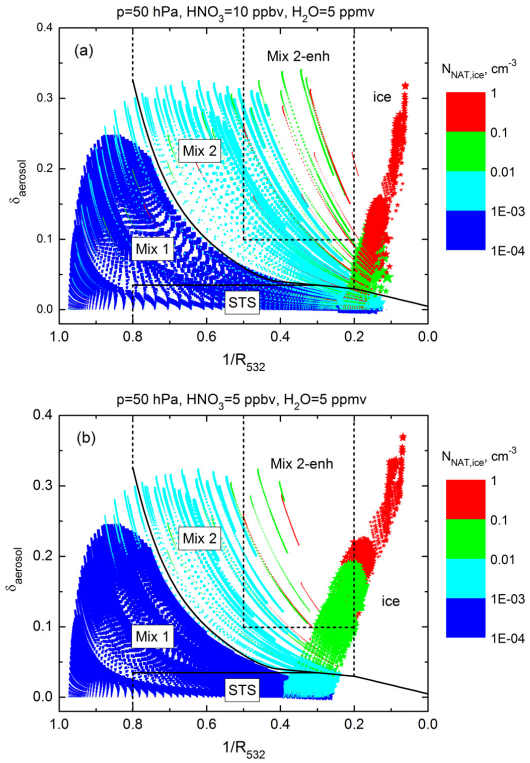

Fig. 11. Theoretical calculations of CALIOP optical signals for various liquid/NAT mixtures and ice computed for the **(a)** standard and **(b)** denitrified conditions. Points are color-coded by particle number densities as indicated in scale on right.

ACPD
12, 24643–24676, 2012

CALIOP polar stratospheric cloud composition classification

M. C. Pitts et al.

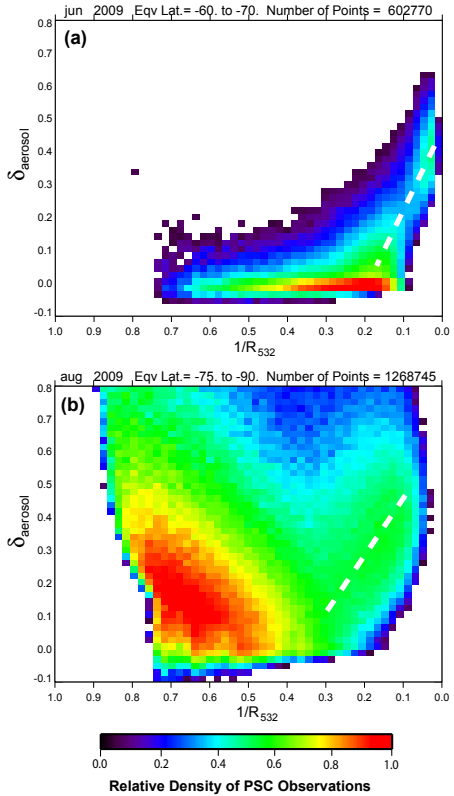

Fig. 12. Distribution of CALIOP PSC observations for **(a)** June and **(b)** August 2009 in selected equivalent latitude bands as indicated at the top of each panel. The colors represent the density of the PSC observations in each bin relative to the maximum. The white dashed lines indicate the axis of the ice PSC observations. The bin size is 0.02 × 0.02 (both unitless).

ACPD
12, 24643–24676, 2012

CALIOP polar stratospheric cloud composition classification

M. C. Pitts et al.

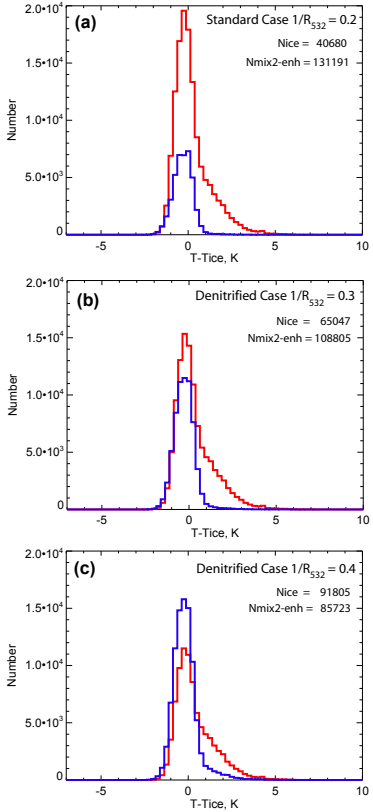

Fig. 13. PDFs of ice (blue) and Mix2-enh (red) PSC observations in the 75° S–90° S equivalent latitude band for August 2009 as a function of $T - T_{ice}$ using an ice/mix2-enh boundary of **(a)** $1/R_{532} = 0.2$, **(b)** $1/R_{532} = 0.3$, and **(c)** $1/R_{532} = 0.4$.

ACPD
12, 24643–24676, 2012